Continuing progress of high-order accurate simulation tool for cargo hold fires

Mark Lohry
Princeton University

FAA JUP Meeting
Atlantic City, NJ
21-22 Jan 2016

Outline

Motivation

- FAA requirement for alarms to go off within 60 seconds of fire ignition.
- Several different detection methods are generally used together, e.g. temperature, smoke/particulate, radiation, optical
- Their effectiveness is determined by the dynamics of a particular fire and their relative position.
- Accurate prediction of fire-induced flow in a cargo hold is a necessary first step to predicting detection capabilities.
- More reliable detection capabilities could potentially reduce false alarms.

Motivation

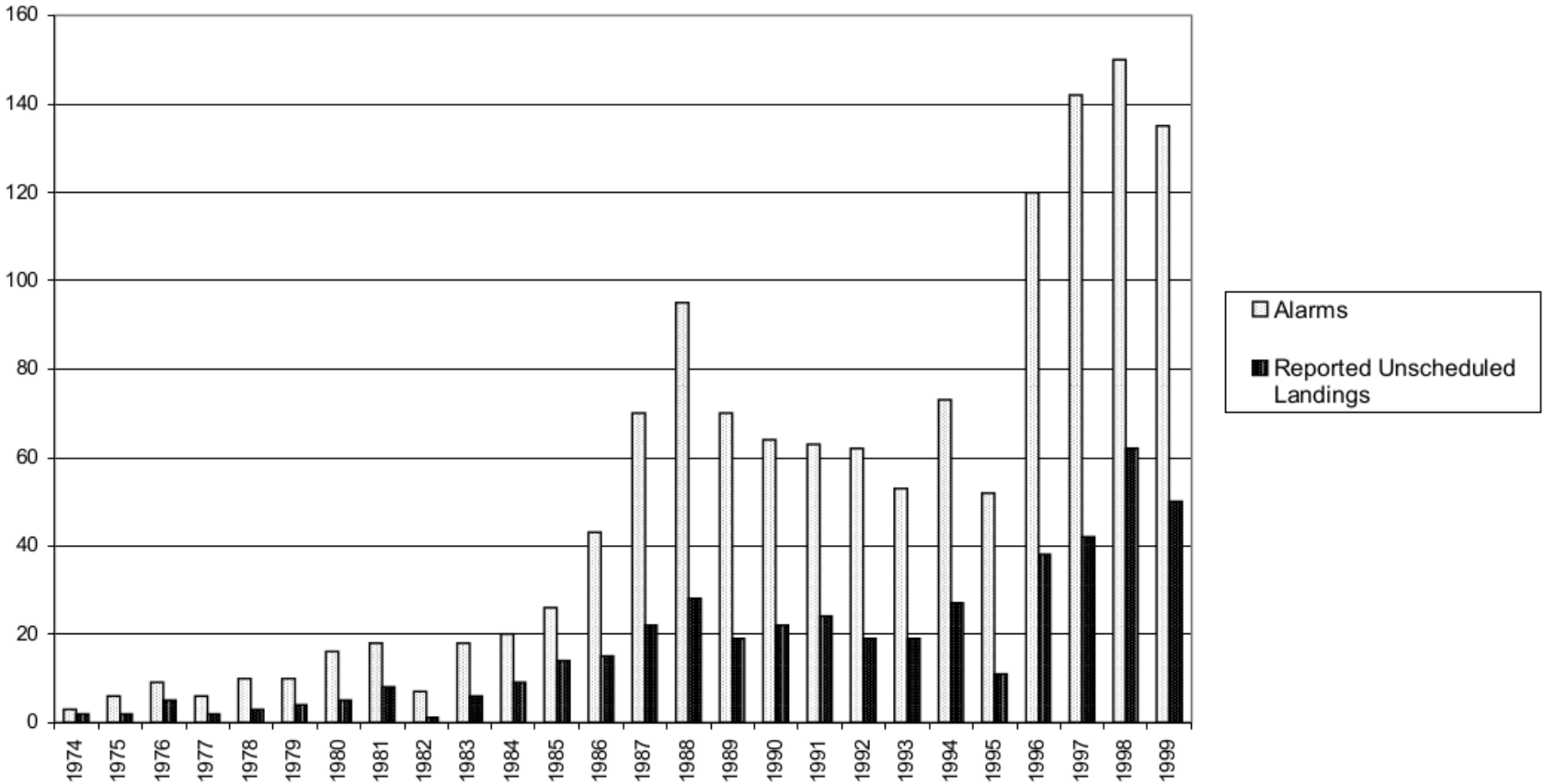

Figure : Unscheduled landings due to cargo compartment false alarms, *Aircraft Cargo Compartment Smoked Detector Alarm Incidents on U.S.-Registered Aircraft, 1974-1999, David Blake*

Motivation

200-to-1 ratio of false alarms in 1995-1999.

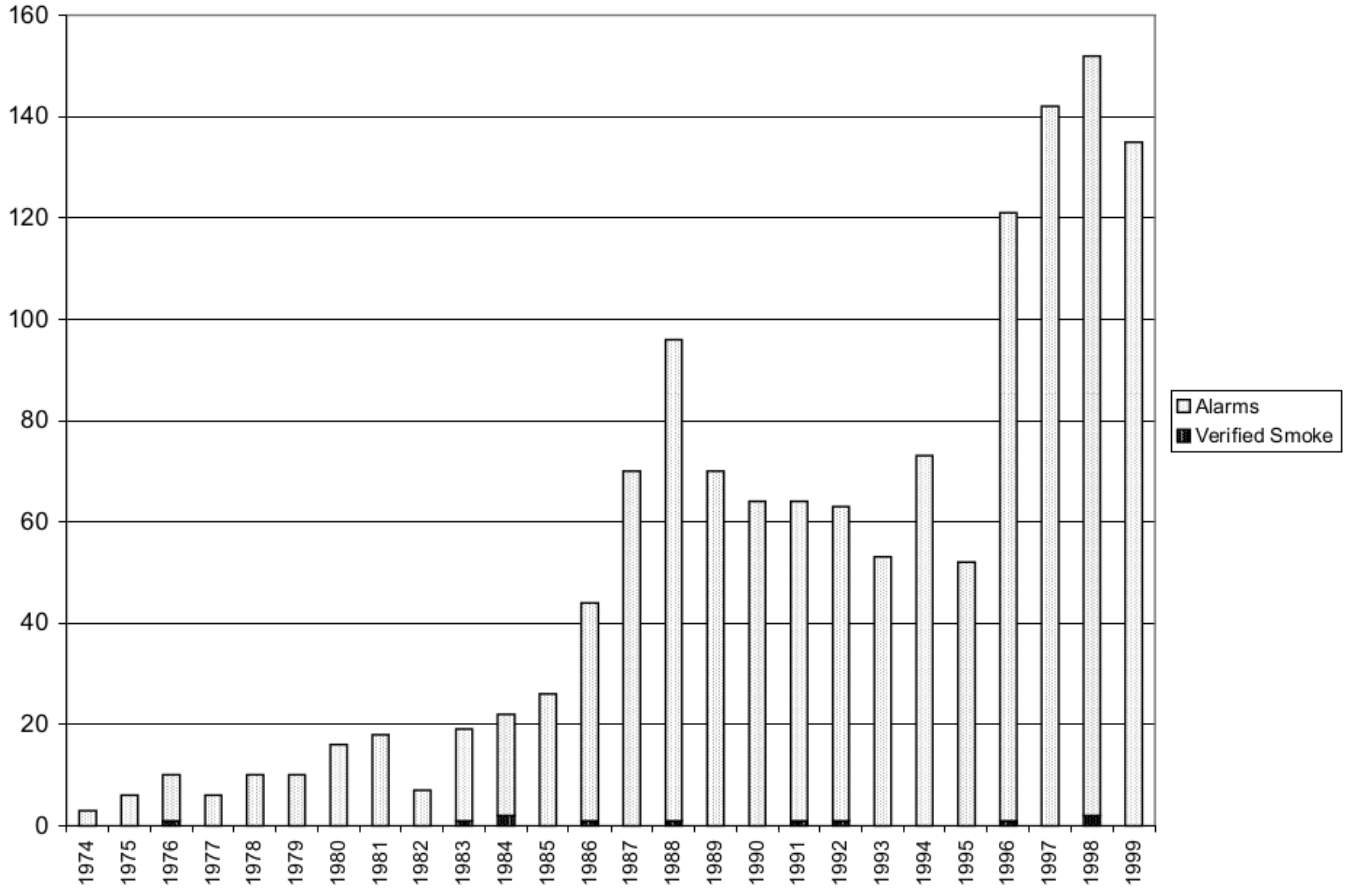

Figure : Number of alarms and number of verified smoke sources, *Aircraft Cargo Compartment Smoked Detector Alarm Incidents on U.S.-Registered Aircraft, 1974-1999, David Blake*

B707 cargo geometry

- Experimental and computational data for B707 cargo fires available from work at Sandia and FAA Tech center.
- Current goal is to perform a direct comparison of those results with our new solver.

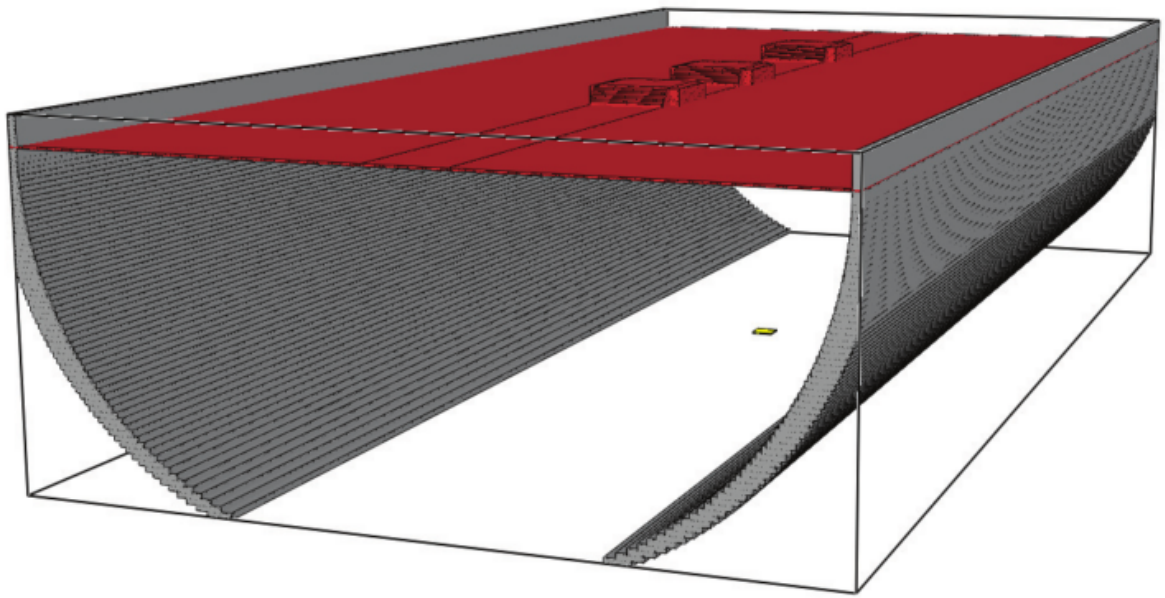

Figure : B707 cargo hold geometry.

Fire-induced fluid dynamics

- Detailed simulation of the combustion process is expensive and unnecessary; the large scale dynamics are primarily determined by the amount of heat release, its position, and the geometry.
- Commonly used models apply a heat source and input of reaction products (CO, CO2, etc.)

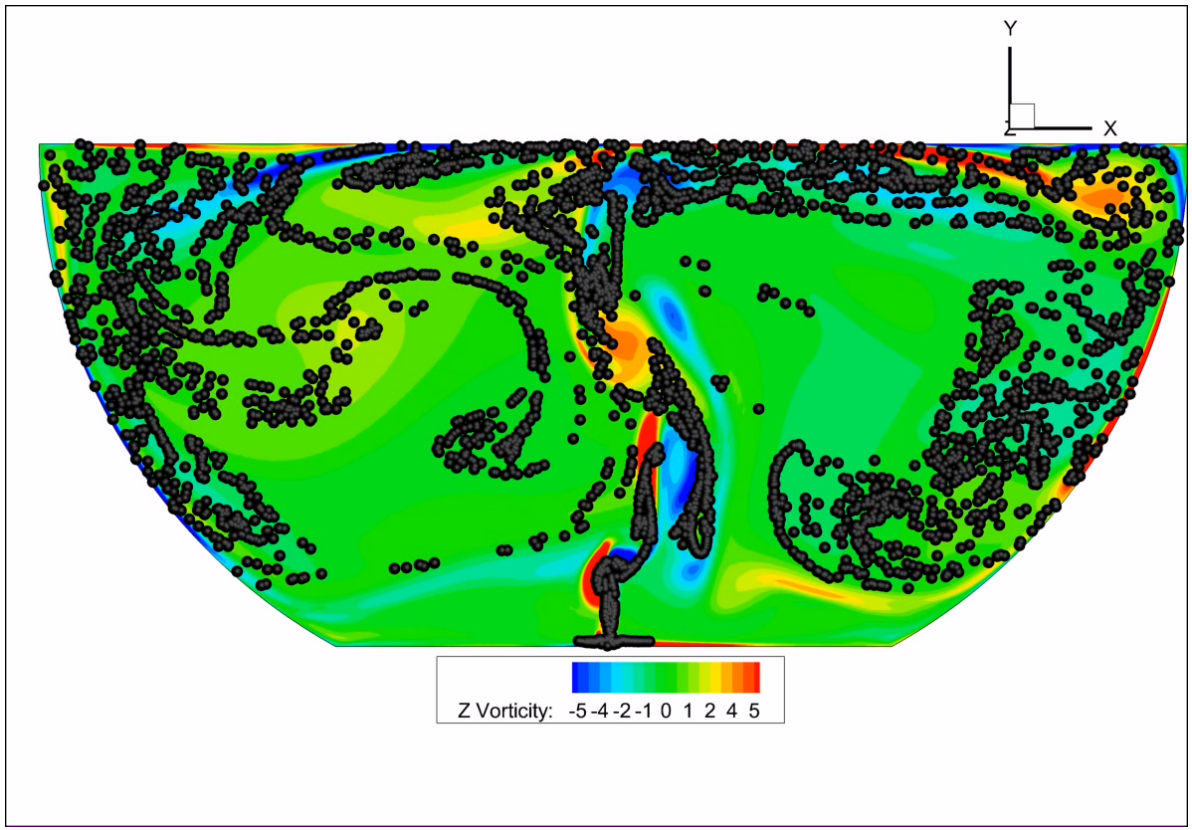

Figure : Flow driven by an enclosed heat source.

Simulation challenges

Simulating a single fire case is relatively straightforward, but of limited utility. There are several **uncertainties** to address:

- Initial position, size, and strength of a fire is unknown.
- Cargo hold geometry varies considerably depending on contents.

Simulation needs:

- Complex geometries: must handle complex boundary conditions accurately.
- Fast: uncertainty quantification will require a large number of simulations.
- Accurate: must accurately simulate vorticity-dominated turbulent flows for transport prediction.

Available tools

FDS: NIST's Fire Dynamics Simulator.

- **Pros:**
  - Purpose-built for smoke and heat transport from fires using large eddy simulation.
  - Combustion and radiation models.
  - Built-in post-processing tools related to smoke transport.
- **Cons:**
  - Handles complex boundaries with Cartesian cut cells: inaccurate for anything but rectangles.

OpenFOAM

- **Pros:**
  - Similar combustion and radiation models to FDS, with additional thermodynamic models.
  - Handles arbitrary body-fitted meshes.
  - Wide array of LES models.
- **Cons:**
  - Very slow for large cases.

Fluent

- **Pros:**
  - Well known, full combustion and radiation modeling.
  - Handles arbitrary body-fitted meshes.
  - Wide array of LES models.
- **Cons:**
  - Commercial

All limited to $O(\Delta x^2)$ accuracy.

Clean geometry 2D

- Typical buoyancy-driven flow in 2D cross-section.

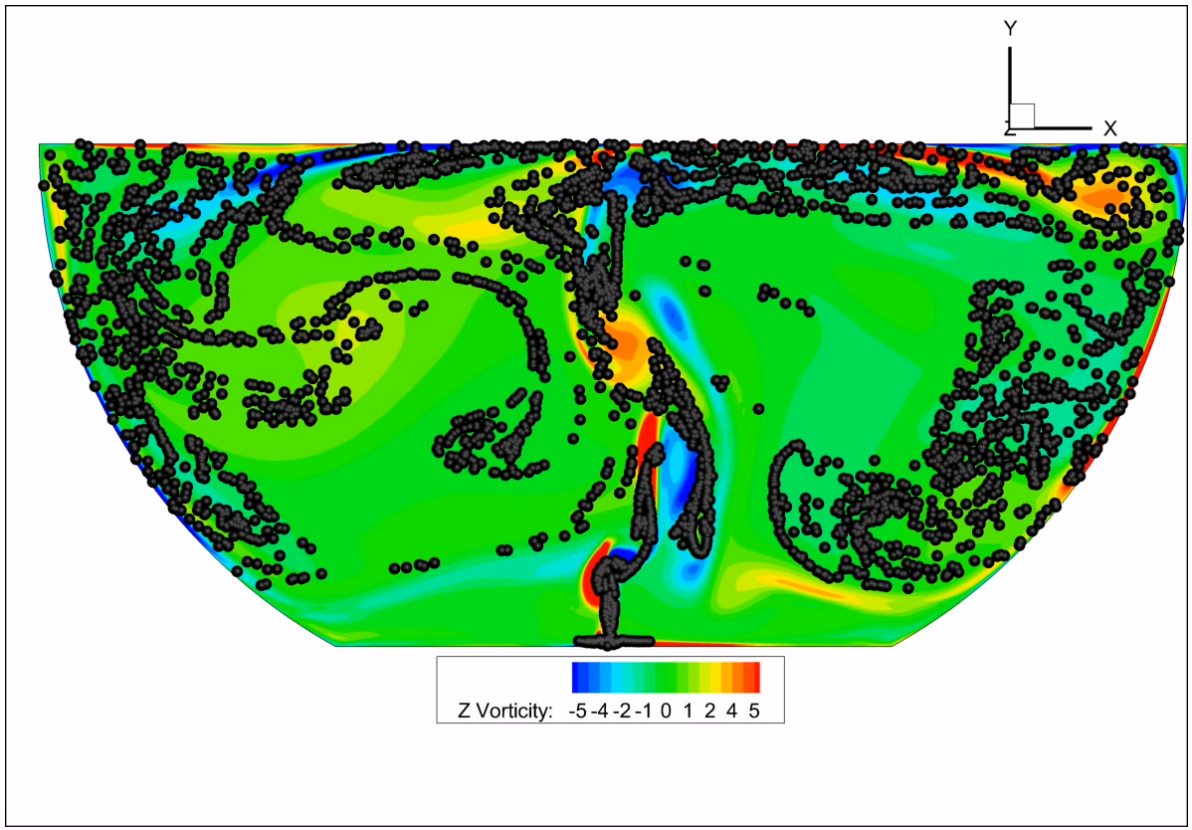

Cluttered geometry 2D

- A real fire is unlikely to happen in an empty cargo hold.
- Including some obstructions changes the flowfield considerably.

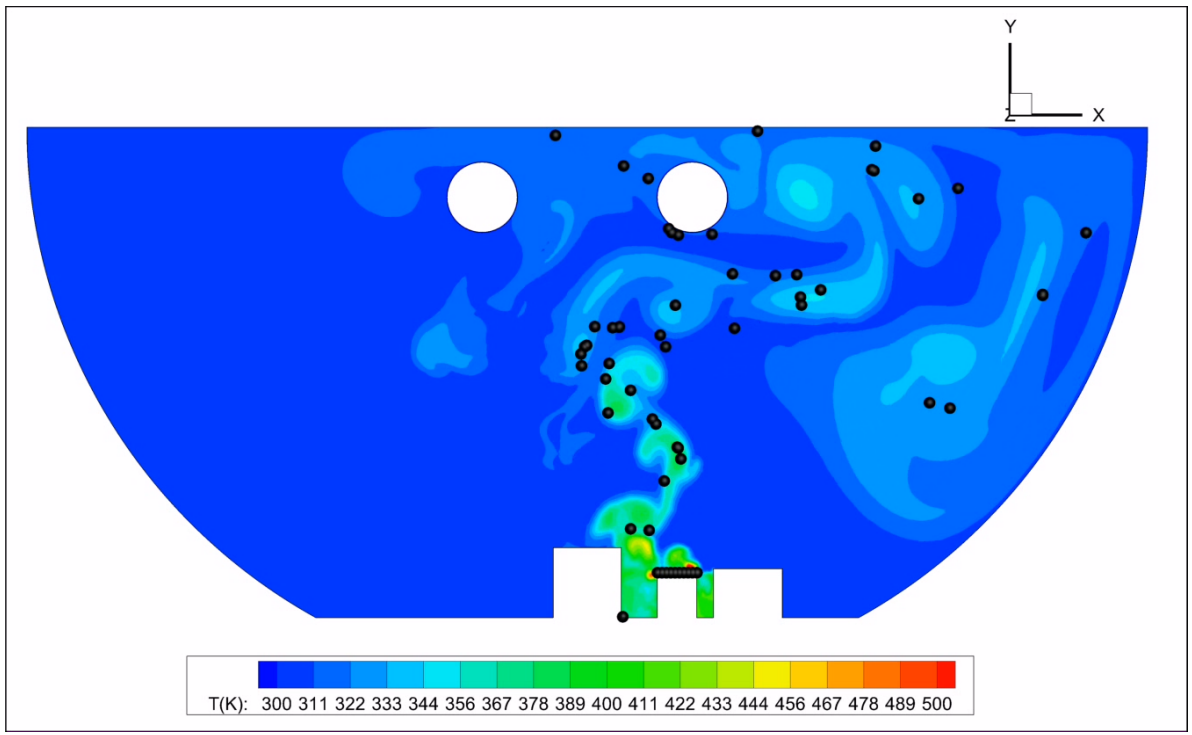

Figure : $t = 5s$ after ignition.

Cluttered geometry 2D

- A real fire is unlikely to happen in an empty cargo hold.
- Including some obstructions changes the flowfield considerably.

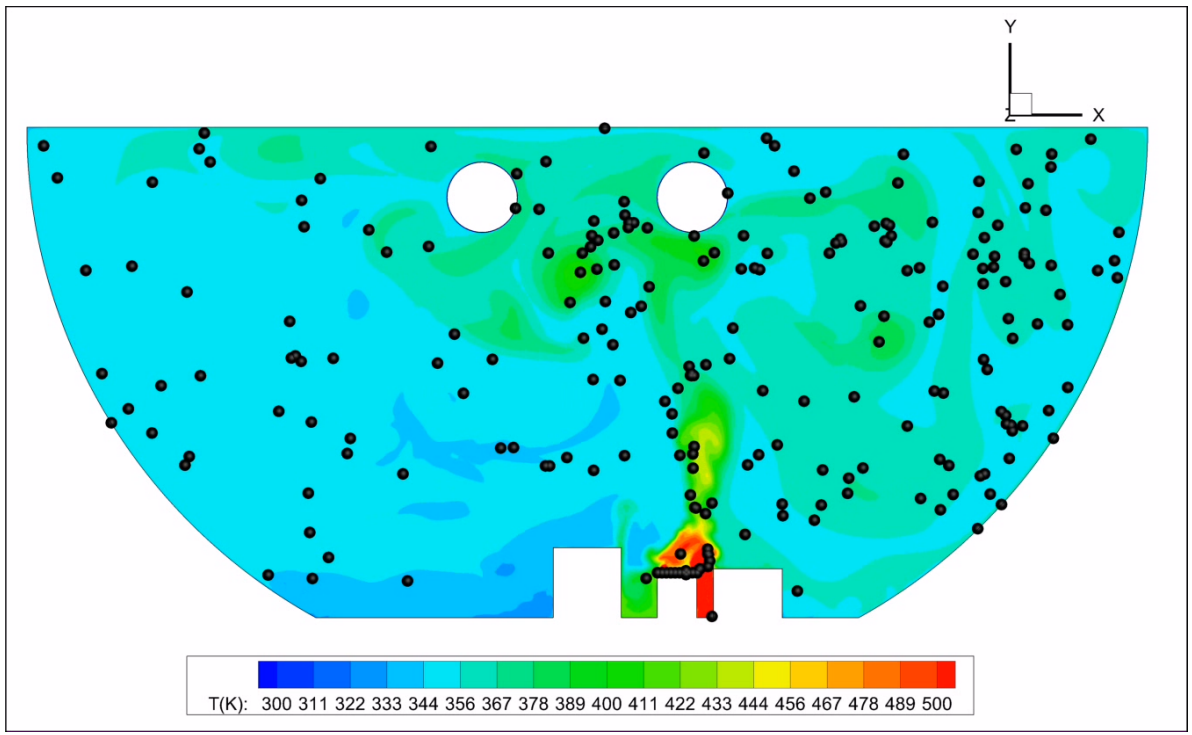

Figure : $t = 20s$ after ignition.

High order accurate CFD

- Even very low intensity fires will have very complex flow phenomena poorly captured by low-order CFD methods.

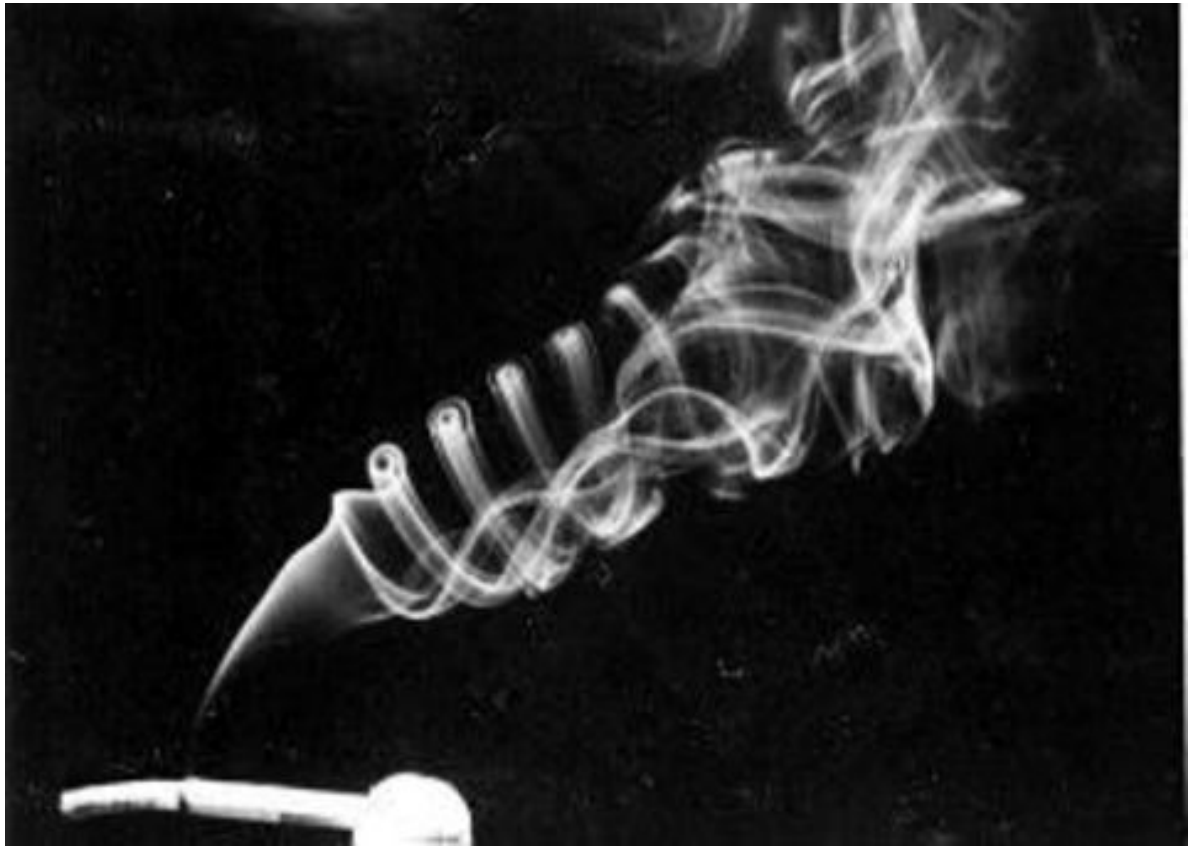

Figure : Instability of smoke from a cigarette, *Perry & Lim, 1978*

High order accurate CFD

Order of accuracy in finite differences:

$$\begin{aligned}
\frac{du}{dx} &\approx \frac{u(x+\Delta x)-u(x)}{\Delta x} + O(\Delta x) \\
\frac{du}{dx} &\approx \frac{u(x)-u(x-\Delta x)}{\Delta x} + O(\Delta x) \\
\frac{du}{dx} &\approx \frac{u(x+\Delta x)-u(x-\Delta x)}{2\Delta x} + O(\Delta x^2)
\end{aligned} \tag{1}$$

- Error scales like $\sim O(\Delta x^n)$ for order n.
- For a 1^{st} order method, halving the grid spacing reduces error by $\sim 1/2$.
- For a 4^{th} order method, halving the grid spacing reduces error by $\sim 1/16$.

High order accurate CFD

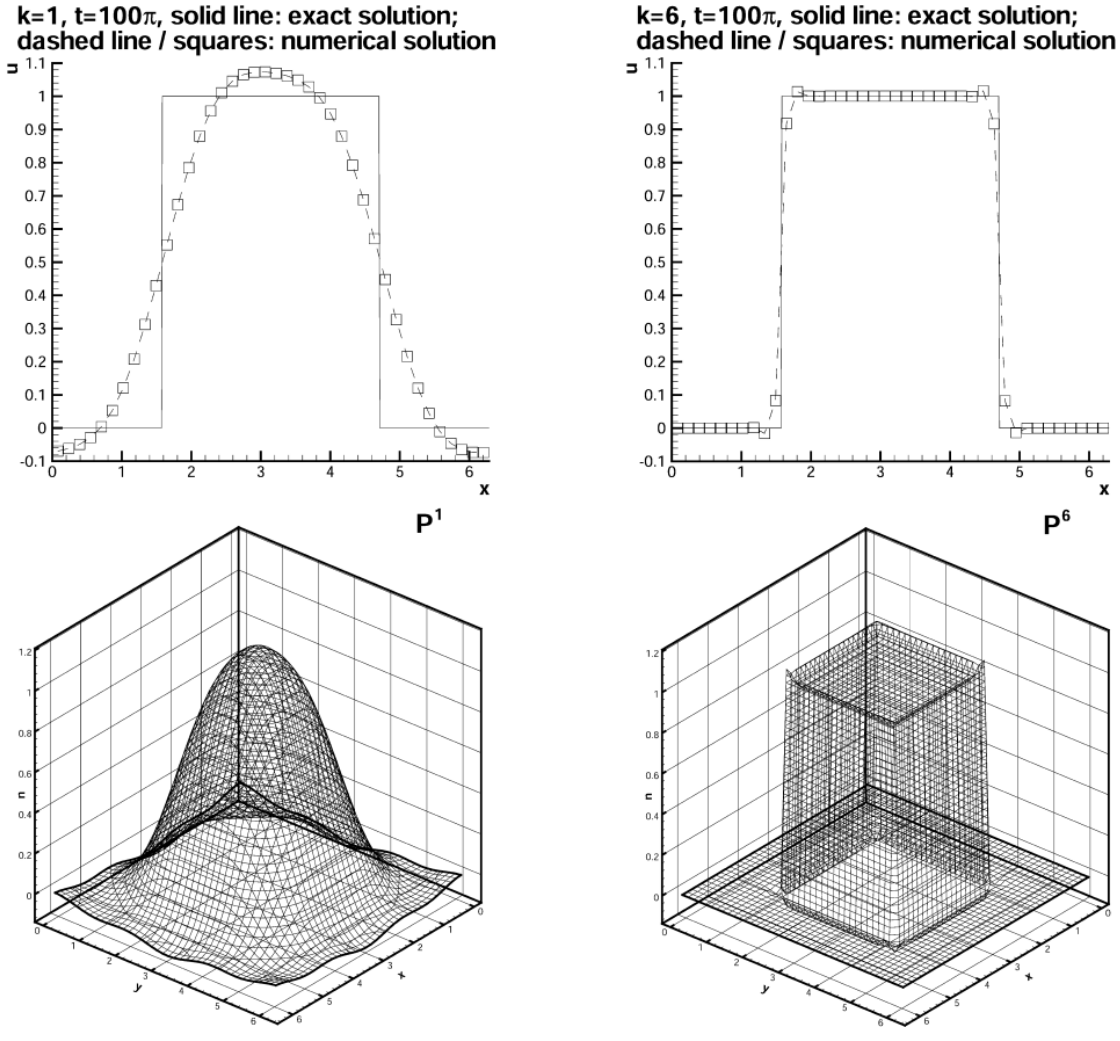

Figure : Linear advection problem, *Cockburn & Shu, 2001*

High order accurate CFD

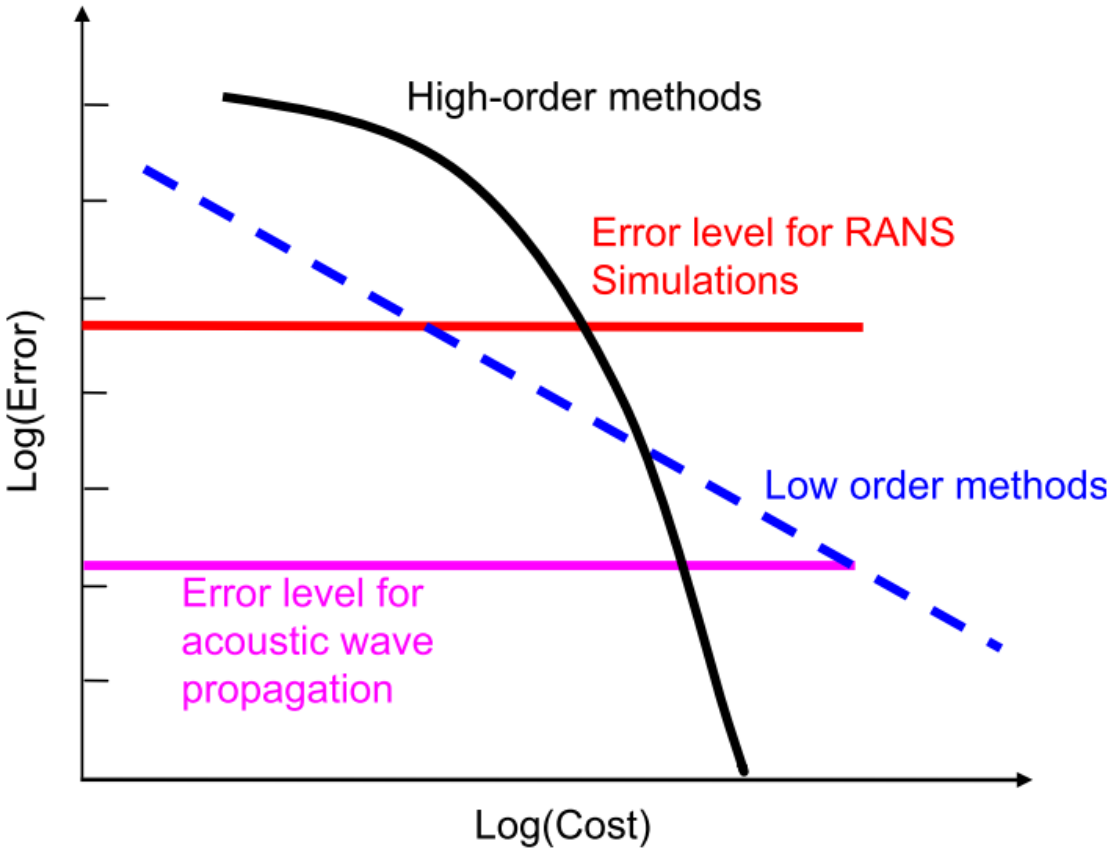

Figure : Generic error vs cost plot, *Wang, 2007*

Discontinous Galerkin

- Traditional 2nd-order accurate methods assume linear functions within cell volumes.
- Discontinuous Galerkin allows arbitrarily high-order accuracy by projecting governing equations onto some polynomial subspace. *DG in a nutshell:*

Conservation law:
$$\frac{\partial \mathbf{u}}{\partial t} + \nabla \cdot \mathbf{f}(\mathbf{u}) = 0$$

Integrate with a test function:
$$\int_V \frac{\partial \mathbf{u}}{\partial t} \phi_j \, dV + \int_V \nabla \cdot \mathbf{f}(\mathbf{u}) \phi_j \, dV = 0$$

Integrate by parts:
$$\int_V \frac{\partial \mathbf{u}}{\partial t} \phi_j \, dV - \int_V \nabla \phi_j \cdot \mathbf{f} \, dV + \oint_S \phi_j \hat{\mathbf{f}} \cdot \hat{\mathbf{n}} \, dS = 0$$

Approximate $\mathbf{u} \approx \sum \mathbf{u}_i \phi_i$:
$$\int_V \frac{\partial \mathbf{u}_i \phi_i}{\partial t} \phi_j \, dV - \int_V \nabla \phi_j \cdot \mathbf{f}_i \phi_i \, dV + \oint_S \phi_j \hat{\mathbf{f}}_i \phi_i \cdot \hat{\mathbf{n}} \, dS$$
$$\mathbf{M}_{ij} \frac{d\mathbf{u}_i}{dt} = \int_V \nabla \phi_j \cdot \mathbf{f}_i \phi_i \, dV + \oint_S \phi_j \hat{\mathbf{f}}_i \phi_i \cdot \hat{\mathbf{n}} \, dS$$

- Compact local support, parallelizable, applicable to complex geometries, and no requirement for periodicity like that used in Fourier methods common in fundamental turbulence studies.

Discontinous Galerkin

Choose the Lagrange polynomials as a basis:

$$l_i(x) \equiv \prod_{\substack{0 \leq m \leq n_i \\ m \neq i}} \frac{x - x_m}{x_i - x_m} \tag{2}$$

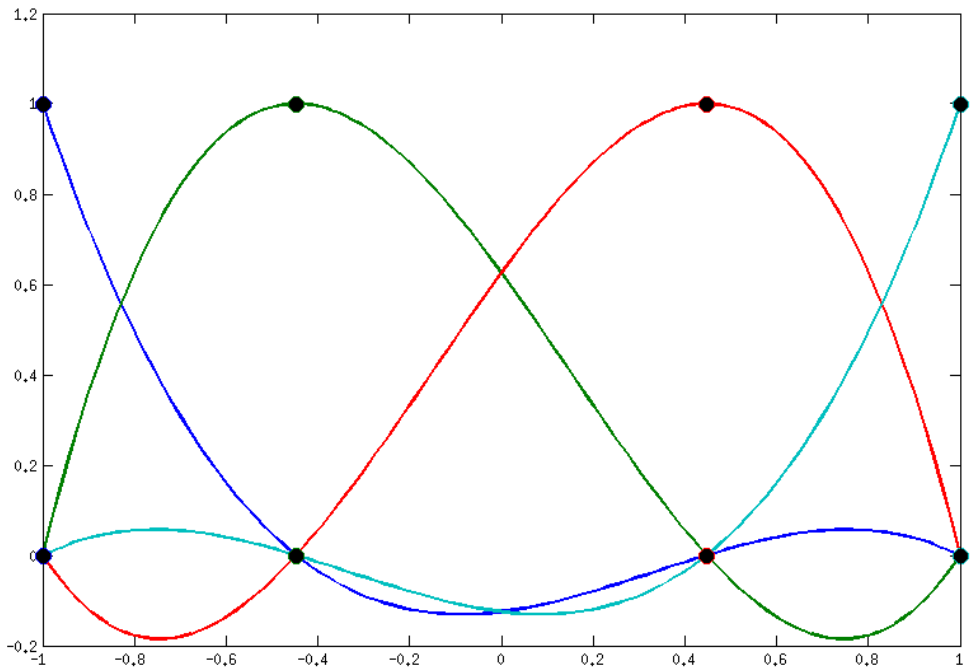

Figure : 3rd order Lagrange polynomials using Chebyshev-Gauss-Lobatto quadrature points.

Discontinuous Galerkin

Extension to 2D and 3D from a tensor product:

$$
\begin{aligned}
l_I(\mathbf{x}) &\equiv l_i(x) l_j(y) l_k(z) \\
&= \left(\prod_{\substack{0 \le m \le n_i \\ m \neq i}} \frac{x - x_m}{x_i - x_m} \right) \left(\prod_{\substack{0 \le m \le n_j \\ m \neq j}} \frac{y - y_m}{y_j - y_m} \right) \left(\prod_{\substack{0 \le m \le n_k \\ m \neq k}} \frac{z - z_m}{z_k - z_m} \right)
\end{aligned} \tag{3}
$$

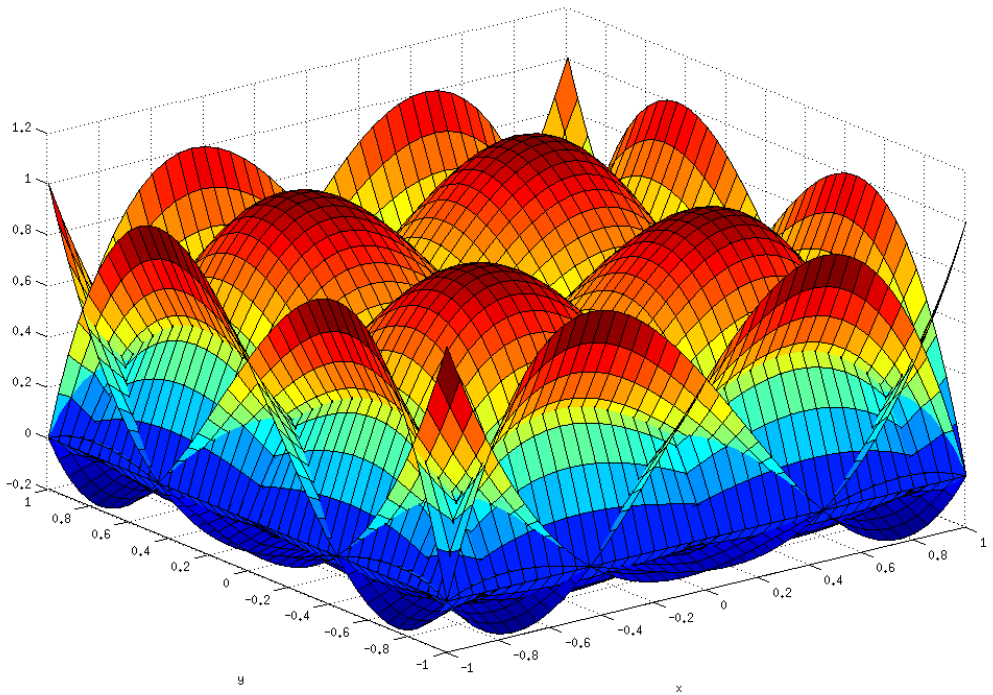

Discontinuous Galerkin - solving the discretized equations

- This ends up with a potentially very large system of ODEs to be solved:

$$\frac{d\mathbf{u}}{dt} = \mathbf{f}(\mathbf{u}, \mathbf{u}', \mathbf{t})$$

- Simplest method for integrating this system in time is the explicit (forward) Euler method:

$$\frac{\mathbf{u}^{n+1} - \mathbf{u}^n}{\Delta t} = \mathbf{f}(\mathbf{u}, \mathbf{u}', \mathbf{t})^{\mathbf{n}}$$

$$\mathbf{u}^{n+1} = \mathbf{u}^n + \Delta t \mathbf{f}(\mathbf{u}, \mathbf{u}', \mathbf{t})^{\mathbf{n}}$$

- Unfortunately, explicit time-stepping for high-order DG is stable only for excessively small Δt,

$$\Delta t = O(\frac{\Delta x}{N^2})$$

where a mesh cell Δx can be very small (boundary layers, small geometric features) and N^2 quickly grows large.

- For any engineering-scale problem, explicit methods are unfeasible for use.

Discontinuous Galerkin - solving the discretized equations

- This requires the use of implicit time-stepping methods, e.g. 1st order backward Euler:

$$\mathbf{u}^{n+1} = \mathbf{u}^{n} + \Delta t \mathbf{f}(\mathbf{u}, \mathbf{u}', \mathbf{t})^{\mathbf{n}} + \mathbf{1}$$

where we now have a set of non-linear equations to solve for u^{n+1}.

- Task is to solve the very large non-linear system at each time step:

$$\mathbf{F}(\mathbf{u}) = 0$$

- Newton's method for this problem derives from a Taylor expansion (Knoll/Keyes 2004):

$$\mathbf{F}(\mathbf{u}^{\mathbf{k+1}}) = \mathbf{F}(\mathbf{u}^{\mathbf{k}}) + \mathbf{F}'(\mathbf{u}^{\mathbf{k}})(\mathbf{u}^{\mathbf{k+1}} - \mathbf{u}^{\mathbf{k}})$$

resulting in a sequence of linear systems

$$\mathbf{J}(\mathbf{u}^{\mathbf{k}})\delta\mathbf{u}^{\mathbf{k}} = -\mathbf{F}(\mathbf{u}^{\mathbf{k}}), \quad \mathbf{u}^{\mathbf{k+1}} = \mathbf{u}^{\mathbf{k}} + \delta\mathbf{u}^{\mathbf{k}}$$

for the Jacobian $\mathbf{J}$.

Discontinuous Galerkin - solving the discretized equations

- The linear system $\mathbf{J}(\mathbf{u}^k)\delta\mathbf{u}^k = -\mathbf{F}(\mathbf{u}^k)$ is straighforward enough to write.
- But for these methods $\mathbf{J}$ is a very large sparse matrix which is prohibitively expensive to actually compute and store.
- A mesh of 100,000 4th order cells requires roughly 250GB of memory to store in 64-bit floats.
- A remedy for this is to use a "Jacobian-Free" method based on Krylov subspace iterations (e.g. GMRES, BiCGSTAB), which only require the action of the jacobian in the form of matrix-vector products:

$$\mathbf{K} = \text{span}(\mathbf{J}\delta\mathbf{r}, \mathbf{J}^2\delta\mathbf{r}, \mathbf{J}^3\delta\mathbf{r}, ...)$$

which can be approximated by a finite difference:

$$\mathbf{J}\mathbf{v} \approx [\mathbf{F}(\mathbf{u} + \epsilon\mathbf{v}) - \mathbf{F}(\mathbf{v})]/\epsilon$$

- This enables a solution method for the non-linear system that doesn't require ever explicitly forming the Jacobian, and instead only requires the evaluation of the RHS of the ODE.

Discontinuous Galerkin

1D test case:

$$\frac{d^2u}{dx^2} = -20 + a\phi'' \cos\phi - a\phi'^2 \sin\phi \qquad (4)$$

$$a = 0.5,\ \phi(x) = 20\pi x^3$$

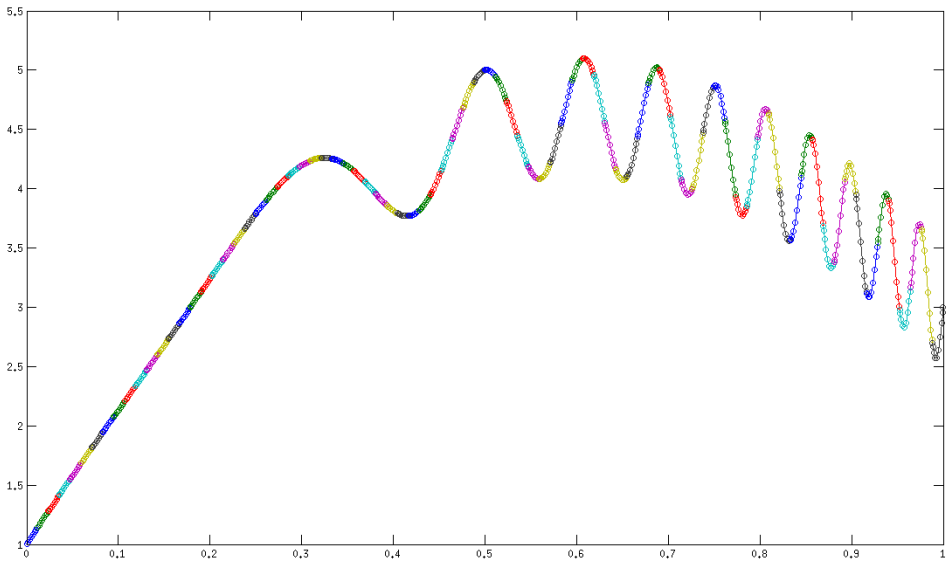

Discontinuous Galerkin

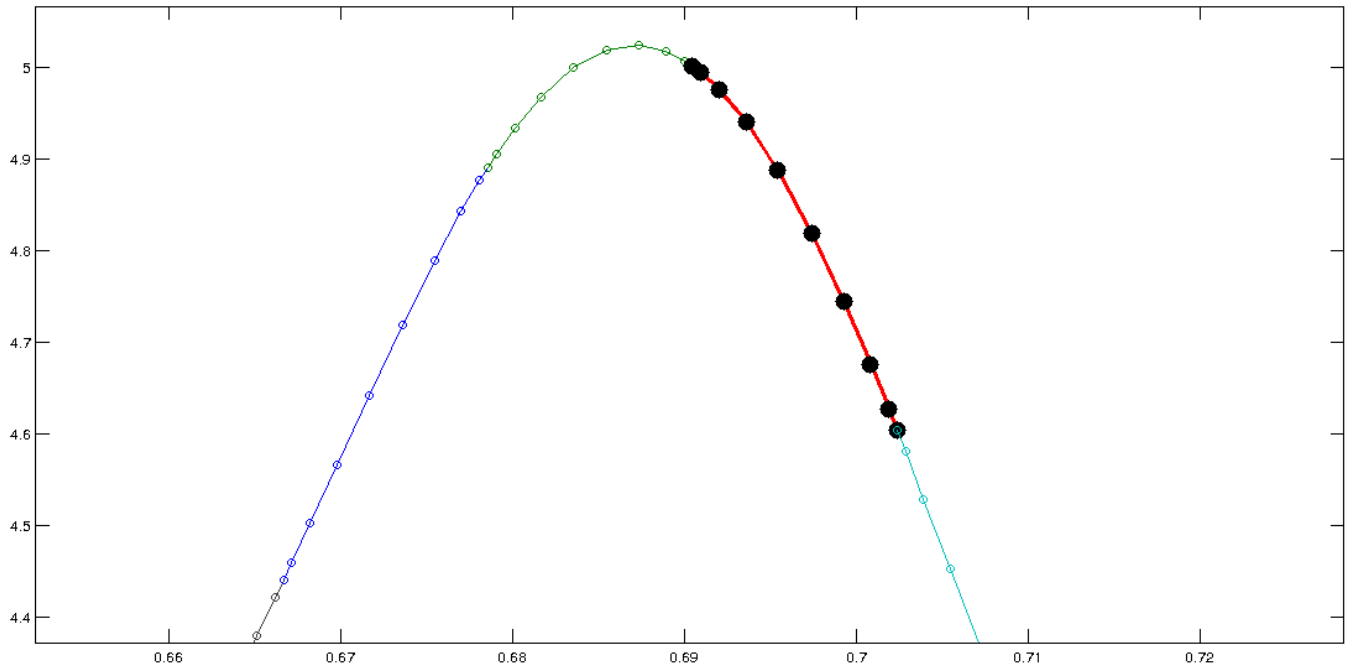

Figure : 9th order polynomial basis.

Discontinuous Galerkin

For an ideal numerical method, computational cost is linearly proportional to the number of unknowns (degrees of freedom).

- *e.g. 10 cells with 10 quadrature nodes compared to 50 cells with 2 quadrature nodes.*

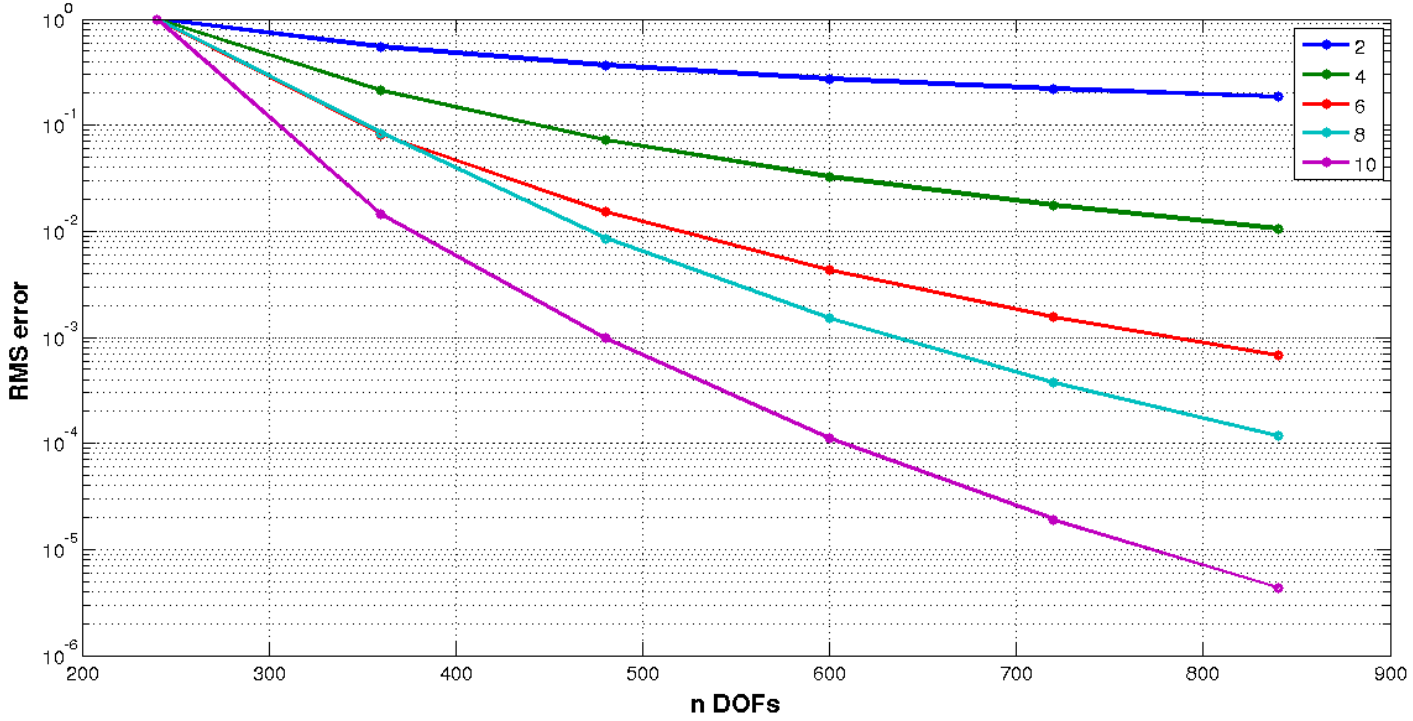

Figure : Error for varying order of accuracy with constant DOFs on 1D test case.

Discontinuous Galerkin

The end result is *hopefully* achieving equivalent accuracy with less computational expense or higher accuracy at similar computational expense compared to traditional finite volume methods.

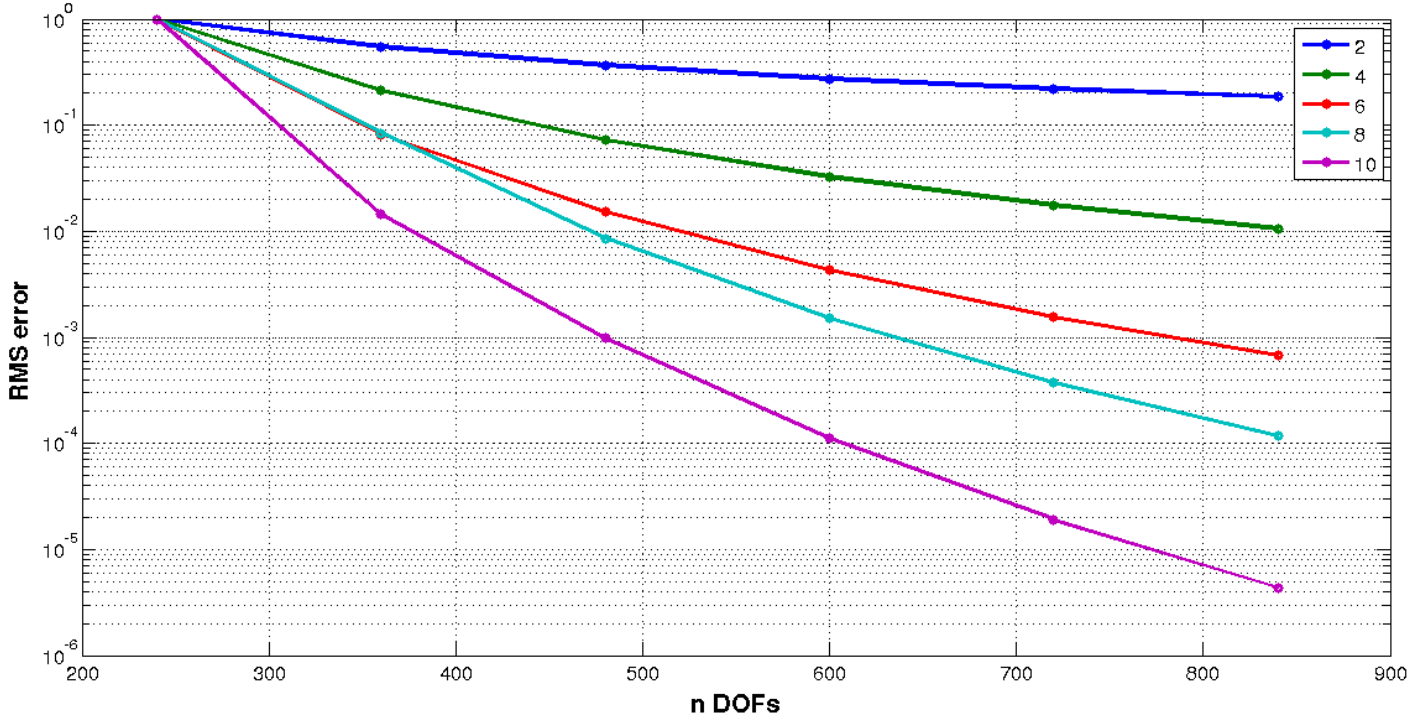

Figure : Error for varying order of accuracy with constant DOFs on 1D test case.

Test case - Isentropic vortex

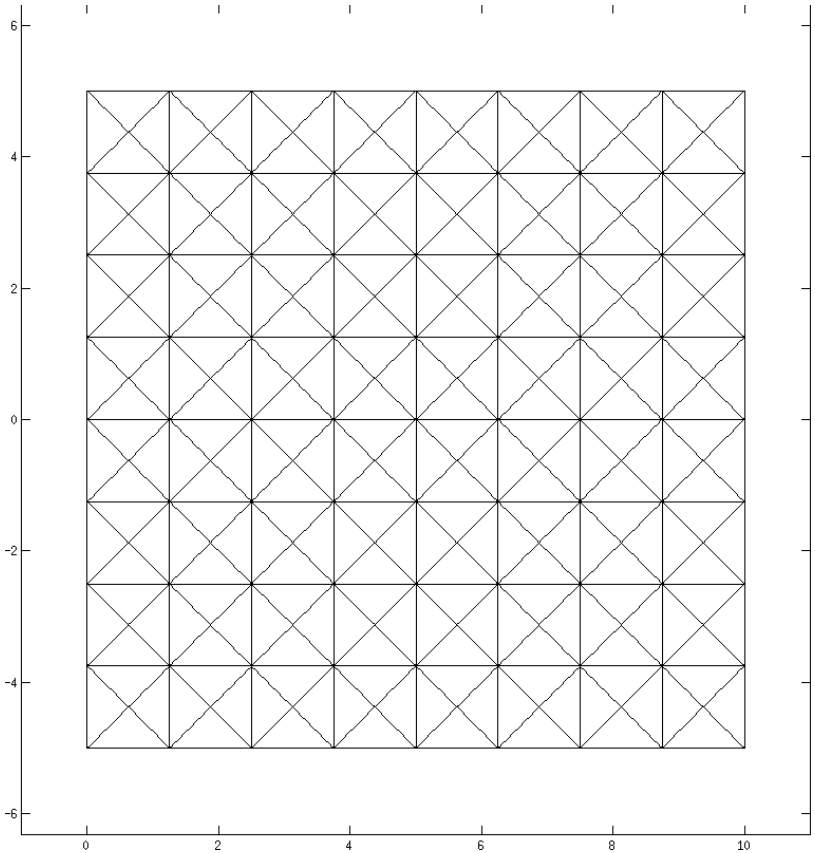

(a) Coarse mesh for vortex case.

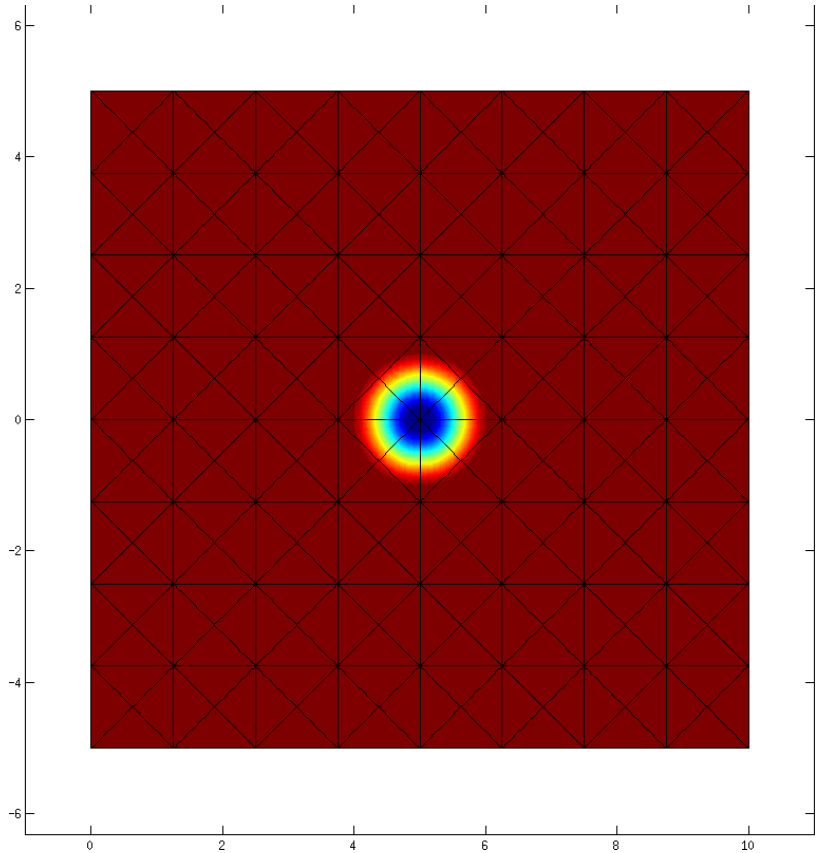

(b) Initial vorticity.

Test case - Isentropic vortex

- Non-dissipative vorticity convection is essential for these simulations.
- Test case of Yee et al (1999) for a convecting vortex is an exact solution for the compressible Euler equations. Free-stream conditions are

$$\rho = 1, u = u_\infty, v = v_\infty, p = 1$$

with an initial perturbation

$$(du, dv) = \frac{\beta}{2\pi} \exp\left(\frac{1 - r^2}{2}\right) [-(y - y_0), (x - x_0)]$$

$$T = 1 - \frac{(\gamma - 1)\beta^2}{8\gamma\pi^2} \exp(1 - r^2)$$

$$\rho = T^{\frac{1}{\gamma - 1}}$$

$$p = \rho^\gamma$$

for vortex center (x_0, y_0), and distance from center $r = \sqrt{(x - x_0)^2 + (y - y_0)^2}$.

Test case - Isentropic vortex - 1st order (c.f. 2nd order FV)

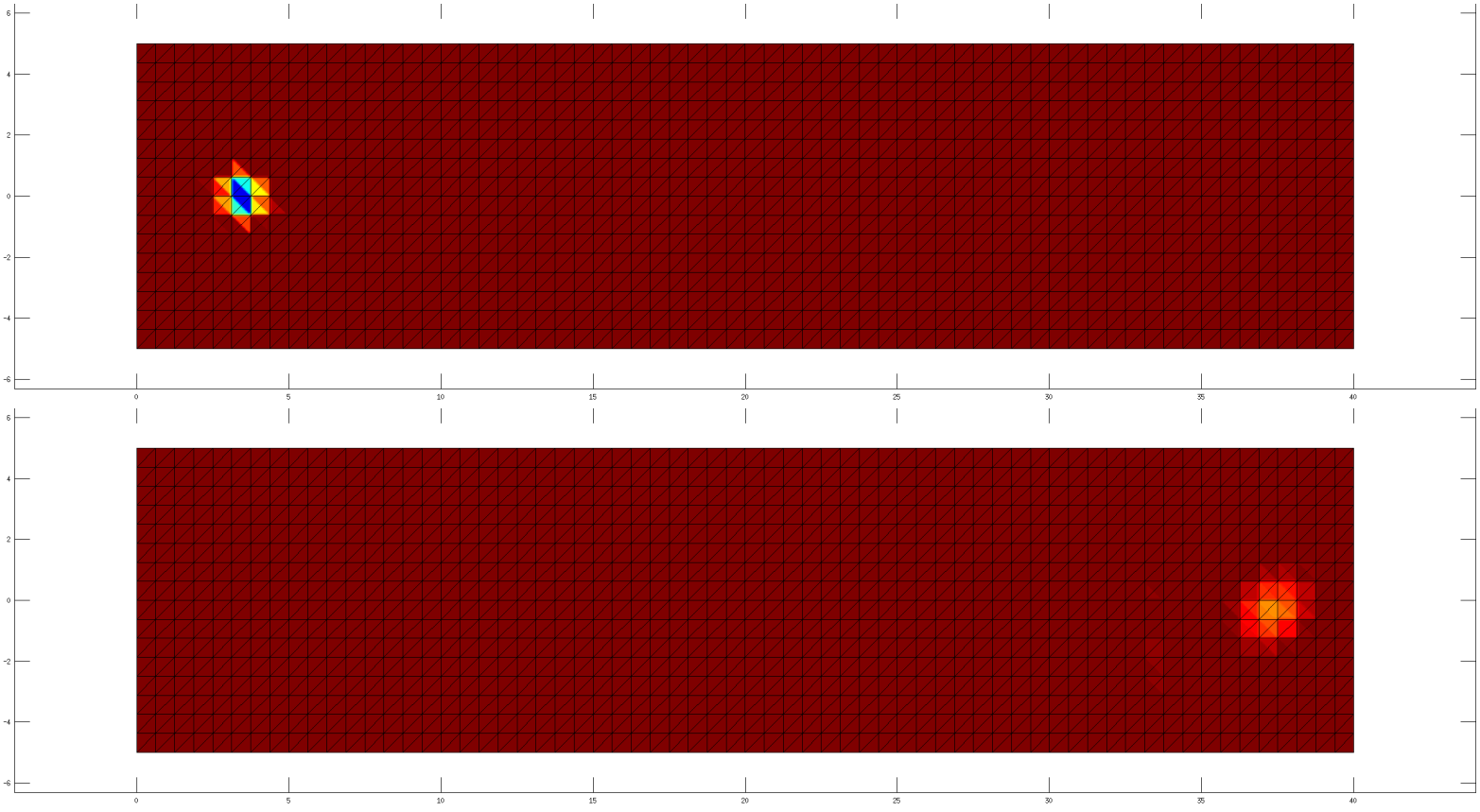

Figure : Vortex transport over 35 characteristic lengths, $O(\Delta x)$.

Test case - Isentropic vortex - 2nd order

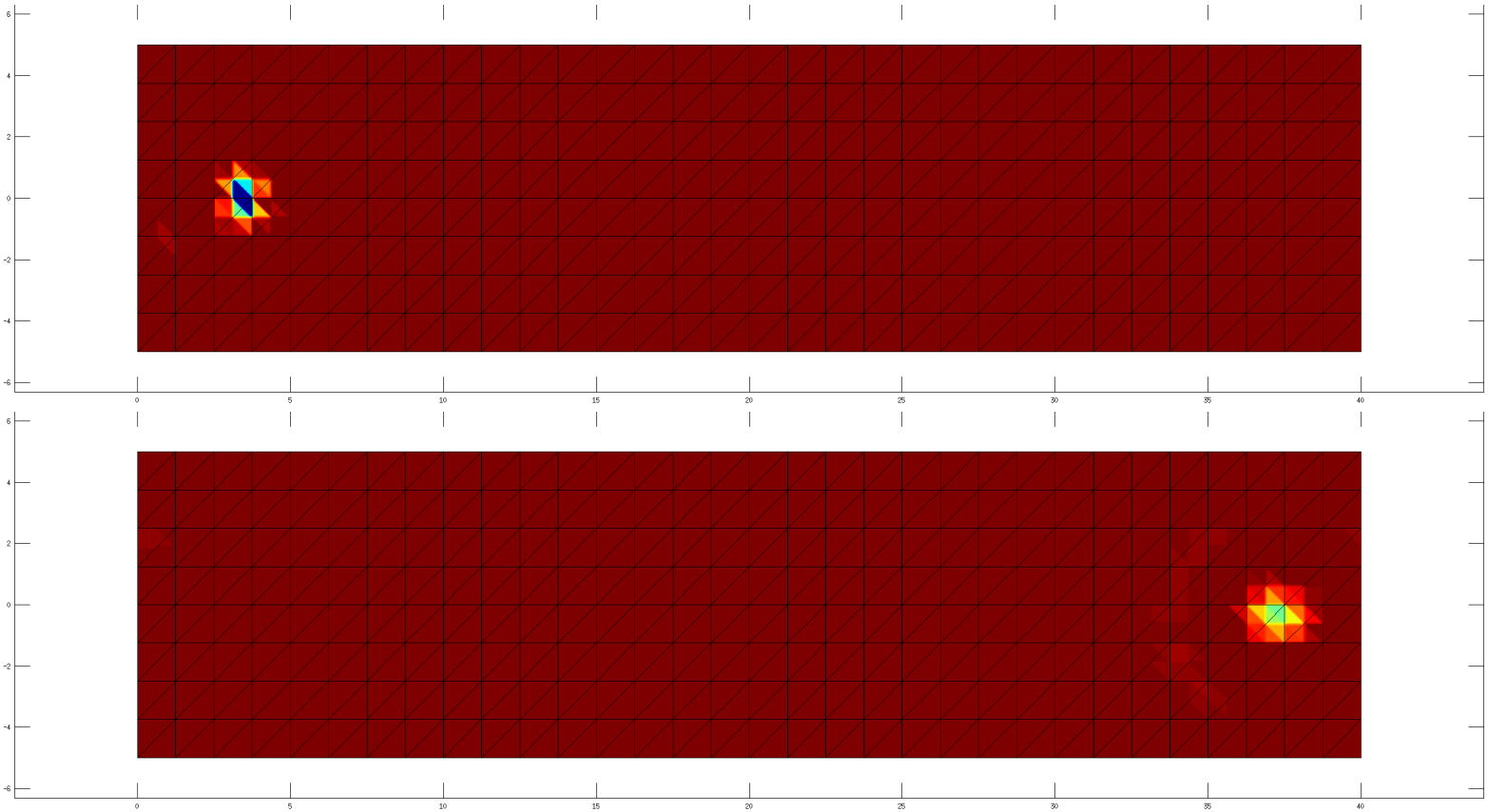

Figure : Vortex transport over 35 characteristic lengths, $O(\Delta x^2)$.

Test case - Isentropic vortex - 3rd order

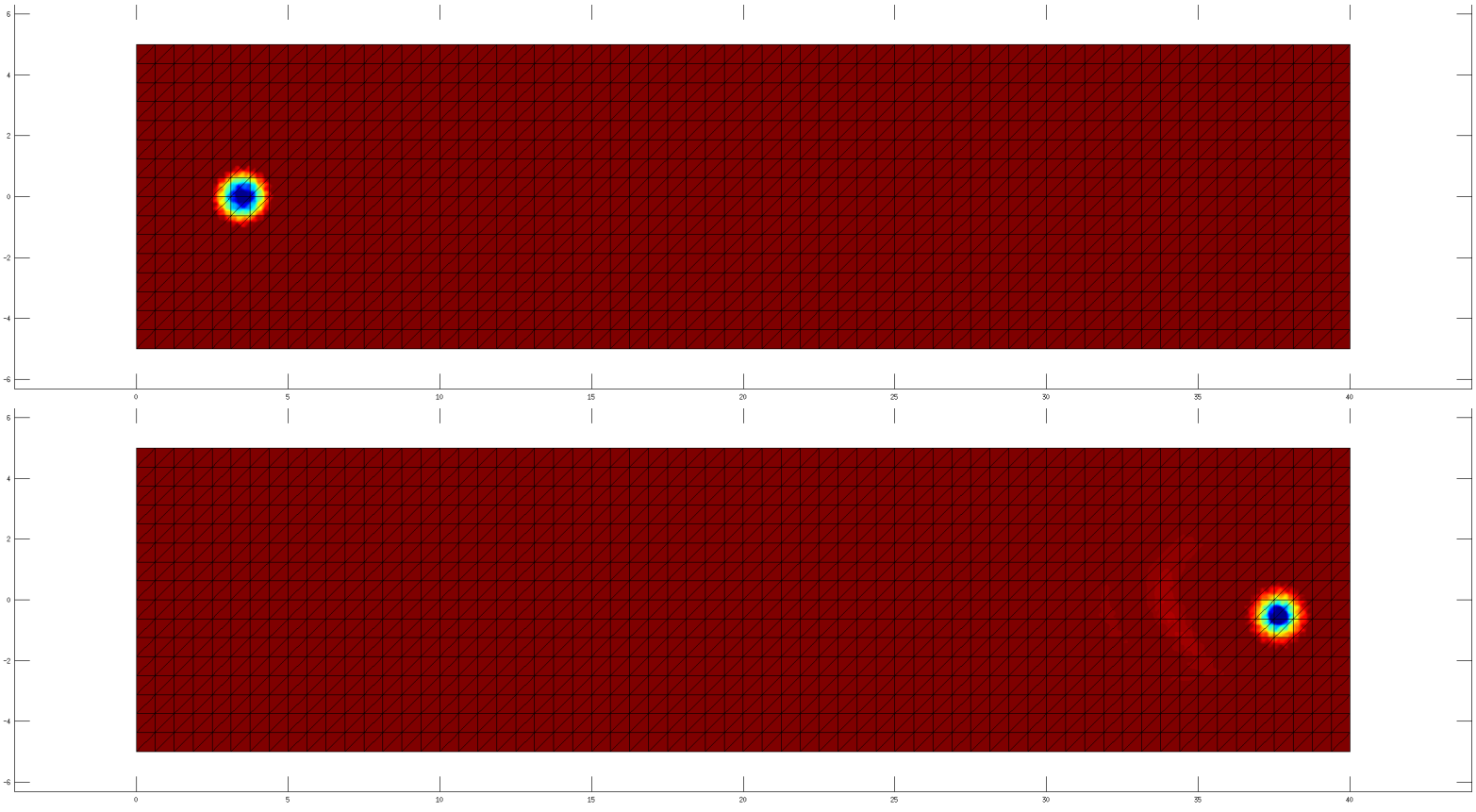

Figure : Vortex transport over 35 characteristic lengths, $O(\Delta x^3)$.

Test case - Isentropic vortex - 4th order

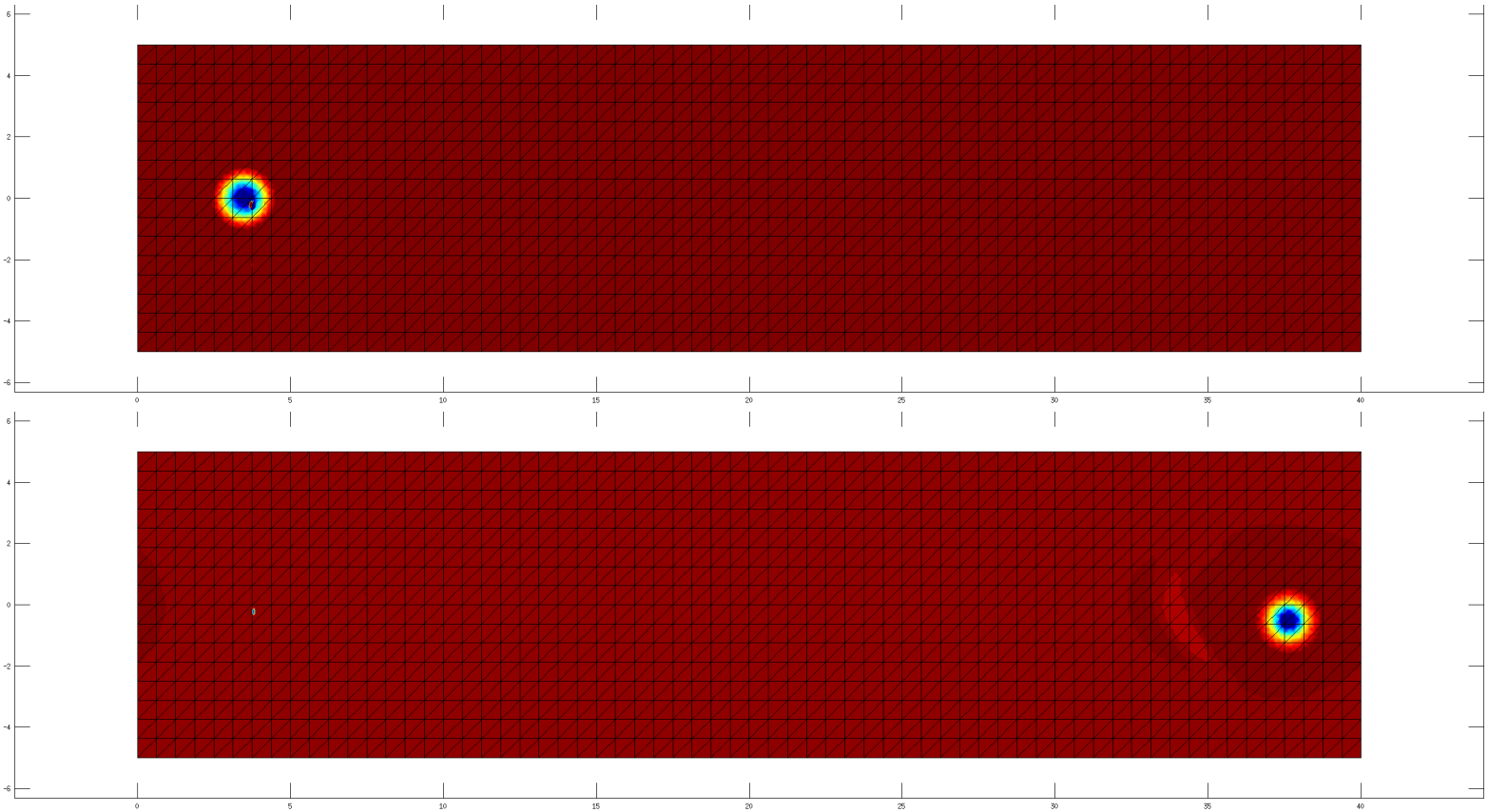

Figure : Vortex transport over 35 characteristic lengths, $O(\Delta x^4)$.

Test case - Isentropic vortex order of accuracy

- L_2 norm of kinetic energy losses for isentropic vortex convection.

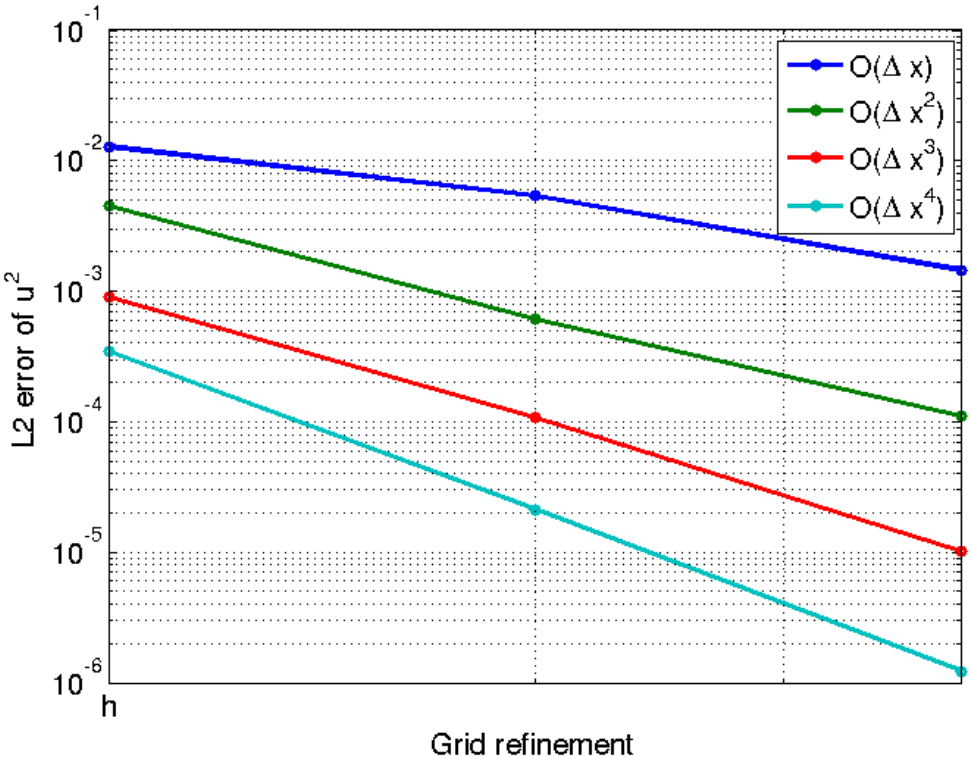

Figure : Solution accuracy versus grid refinement, for levels h, $h/2$, and $h/4$.

Buoyant-driven 2D flow example

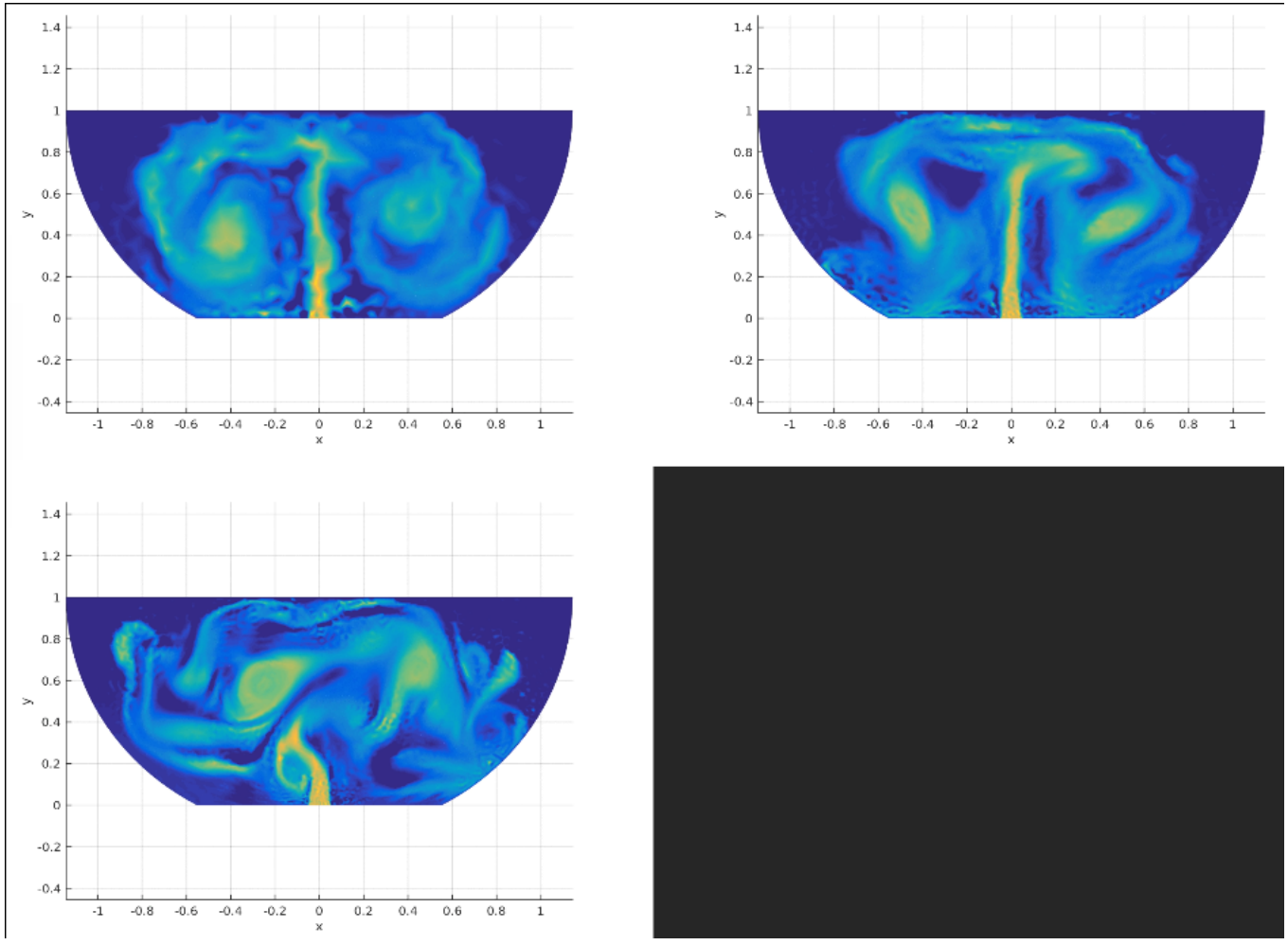

Figure : Order δx, δx^2, δx^3 simulations at $t = 9s$ after ignition.

(video)

AIAA 2016 2D cargo hold results

Uncertainy Quantification for Cargo Hold Fires, DeGennaro, Lohry, Martinelli, & Rowley, *57th AIAA Structures, Structural Dynamics, and Materials Conference*, San Diego CA, Jan. 2016.

- Two objectives of this study:
  - Assess the feasibility of using DG methods for buoyancy-driven flows,
  - Use uncertainty quantification techniques to analyze statistical variations in flows.

Simulation parameters

- The mock fire sources were chosen to vary based on 2 parameters: fire strength and location.
  - Fire location was chosen to vary between the centerline and the far right wall, exploiting the symmetry of the geometry.
  - Fire strength was chosen to vary between a weak, slowly rising plume and a faster rising plume.
- 5×5 parameter sweep performed for these 2 parameters.
- Simulations performed with 3rd order elements (10 nodes per 2D cell) with approximately 1,500 triangular cells, or 15,000 nodes. All boundary conditions are isothermal non-slip walls.

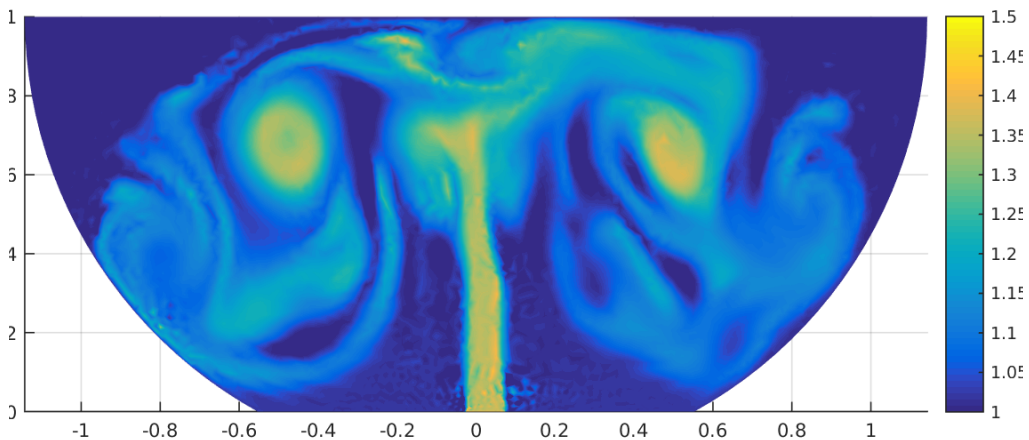

Simulation parameters

- Time evolution of temperature field:

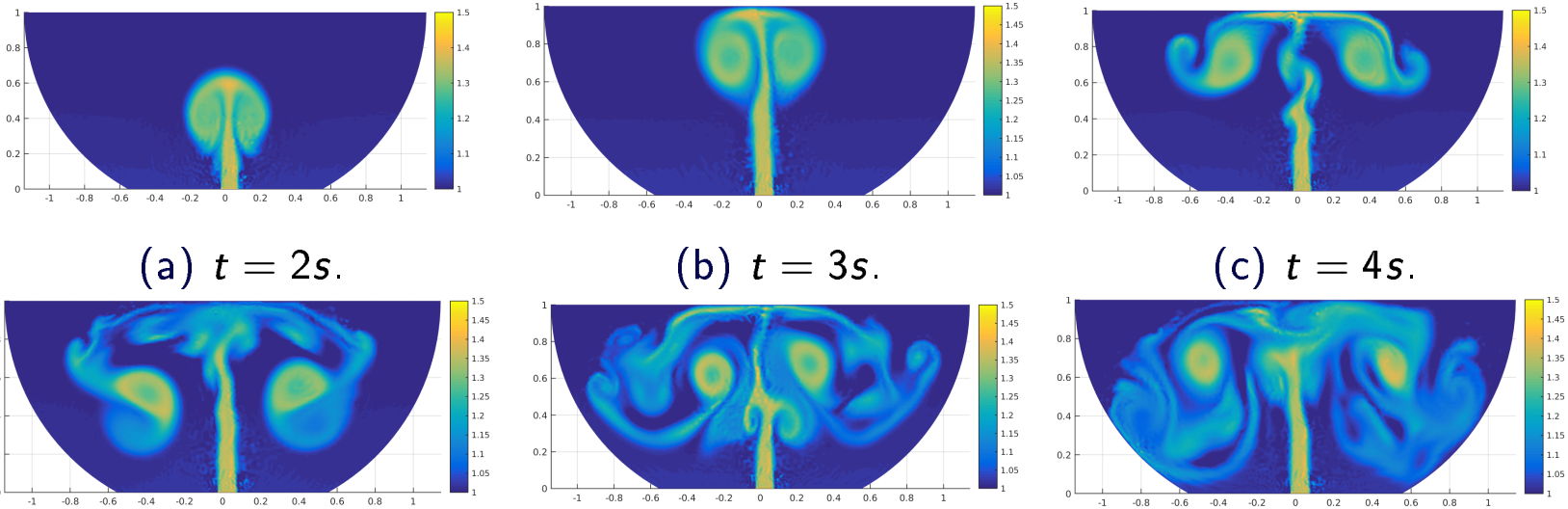

(a) $t = 2s$. (b) $t = 3s$. (c) $t = 4s$.

(d) $t = 5s$. (e) $t = 6s$. (f) $t = 7s$.

Figure : Temperature field time evolution for $T_s = 1.486$, $x_s = 0.024$ case.

Simulation parameters

- Variation of fire source location:

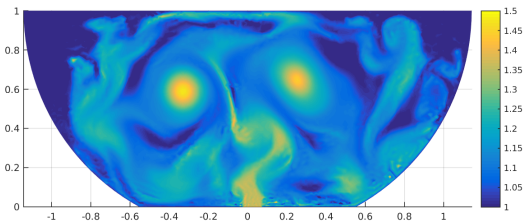

(a) $x_s = 0.024m$.

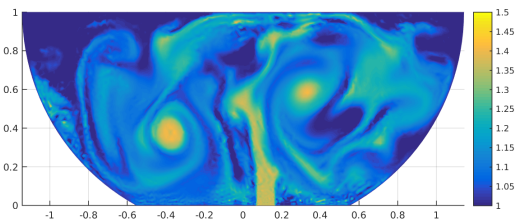

(b) $x_s = 0.116m$.

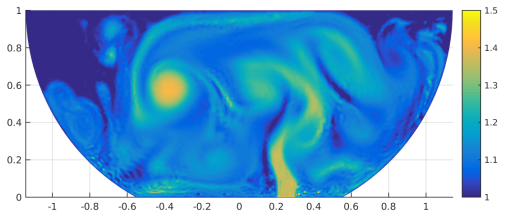

(c) $x_s = 0.262m$.

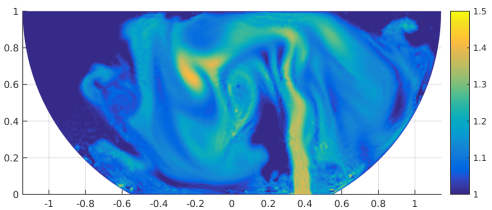

(d) $x_s = 0.387m$.

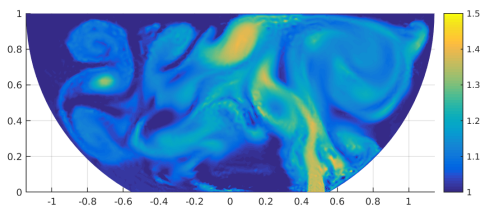

(e) $x_s = 0.480m$.

Figure : Temperature fields for $T_s = 1.486$ source at the 5 source locations, time $t = 10s$ after startup.

Simulation parameters

- Variation of fire source temperature:

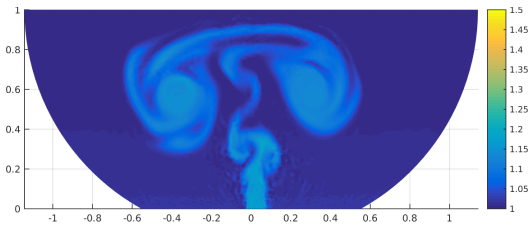

(a) $T_s = 1.214$.

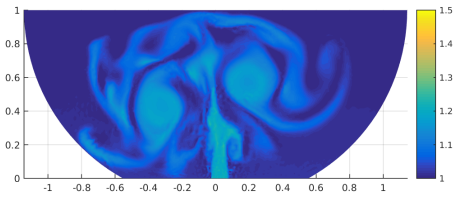

(b) $T_s = 1.269$.

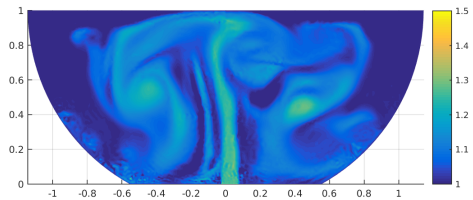

(c) $T_s = 1.350$.

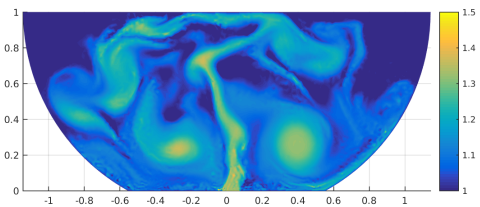

(d) $T_s = 1.431$.

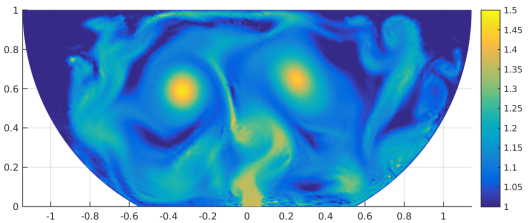

(e) $T_s = 1.486$.

Figure : Temperature fields at $x_s = 0.024m$ for the 5 values of temperature source, time $t = 10s$ after startup.

AIAA 2016 2D cargo hold results

(video)

AIAA 2016 2D cargo hold results

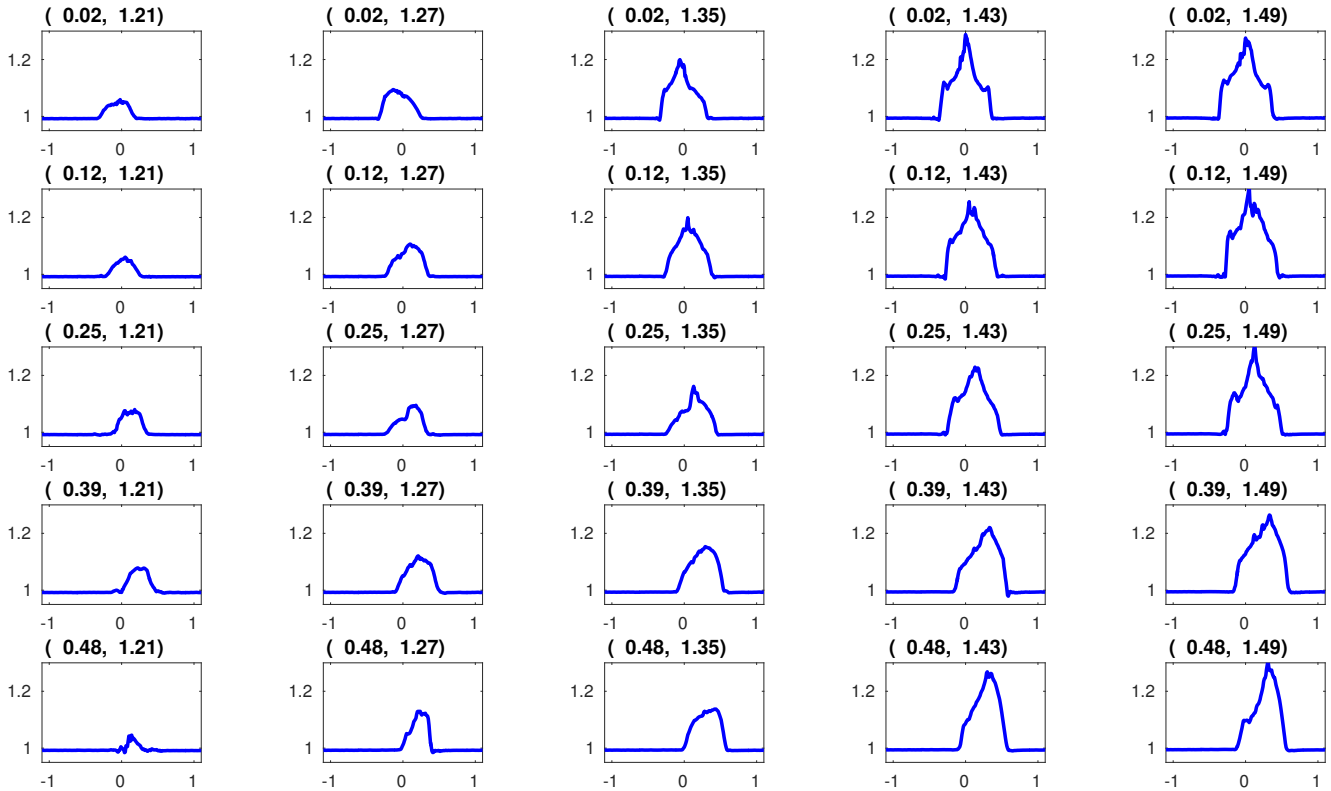

Figure : Time-averaged ceiling temperature distributions collected at the 25 quadrature nodes. Each subtitle corresponds to the parameter pair (x_S, T_S).

Ongoing solver development

2D work completed:

- Established that high-order-accurate discontinuous Galerkin methods can be used for simulating buoyancy-driven flows such as those seen in cargo hold fires, using unstructured meshes suitable for arbitrary geometries.
- Demonstrated the use of these simulations in an uncertainty quantification framework to aid in fire sensor placement.

Current work is on extending this to a 3D solver for full cargo hold simulation:

- Functioning:
  - 3D unstructured flow solver, spatial discretization with arbitrary order of accuracy.
  - Parallel scaling.
  - Jacobian-Free Newton-Krylov for solution of non-linear algebra.
  - Implicit time integration for high order temporal accuracy and large time step stability.
- Work in progress:
  - Full testing of 3D viscous effects.
  - Implementation of Large Eddy Simulation (LES) models.
  - Full cargo hold simulations.
  - Apply Anthony's uncertainty quantification methods for testing range of fire sources in B707 geometry.
  - Direct quantitative comparisons between Fluent and this DG work for validation.

End